AIAA 2005-4532

The Conical Bidirectional Vortex

O. C. Sams, IV and J. Majdalani
Advanced Theoretical Research Center
University of Tennessee Space Institute
Tullahoma, TN 37388

41st AIAA/ASME/SAE/ASEE Joint Propulsion Conference and Exhibit
10–13 July 2005
Tucson, AZ

41st AIAA/ASME/SAE/ASEE Joint Propulsion Conference and Exhibit
10-13 July 2005, Tucson, Arizona

AIAA 2005-4532

The Conical Bidirectional Vortex

Oliver C. Sams IV* and Joseph Majdalani†
University of Tennessee Space Institute, Tullahoma, TN 37388

In this article, a leading order approximation is obtained for the bidirectional vortex in a conical chamber. The model is applicable to both cyclone separators and liquid rocket engines with slowly expanding chamber cross-section. The bulk fluid motion is assumed to be nonreactive, steady, rotational, inviscid, and incompressible. Results are illustrated for several cone divergence angles and chamber aspect ratios. For the limiting case of zero divergence, our results reduce to the known solution obtained for a cyclone in a straight cylinder.

Nomenclature

p	=	normalized pressure, $\overline{p}/(\rho V_{\text{inj}}^2)$
R_0	=	base radius of conical chamber
r	=	normalized radial coordinate, $\overline{r}/R_0$
u	=	normalized velocity, $\overline{u}/V_{\text{inj}}$
V_{inj}	=	tangential injection velocity
z	=	normalized axial coordinate, $\overline{z}/R_0$
ψ	=	normalized streamfunction
ρ	=	density
Ω	=	normalized vorticity
ξ	=	velocity ratio, $u_{\max}/u_{\text{ave}}(z)$

Subscripts and Symbols

$0, 1$	=	leading and first order
r, z, θ	=	radial, axial, or azimuthal component
–	=	the overbar denotes a dimensional quantity

I. Introduction

INTEREST in modeling cyclonic motion has been recently revived, especially in propulsive applications where swirl-driven cyclones have become known for their elevated efficiencies and self-cooling properties. In fact, several types of liquid[1-11] and hybrid[12-20] rocket engines under development today are based on the so-called bidirectional vortex; this bipolar vortex is a cyclone comprising a pair of (outer and inner) coaxial, co-rotating swirling streams that are separated by a spinning wheel known as the mantle. The latter constitutes a rotating, non-translating shear layer along which mass can cross inwardly from the outer, annular vortex to the inner, central core where combustion and mixing are vigorously promoted.

Using cylindrical combustion chambers, analytical mean flow models have been recently advanced by Vyas, Majdalani and Chiaverini[9-11] for the liquid engine application, and by Majdalani and Vyas[12] for the hybrid engine case. Cold flow experimentation using PIV[1,2] and numerical models have also been implemented under both cold[21] and reactive flow conditions[22] and used to guide the design of future vortex engines.

*Former Graduate Student, Department of Mechanical and Industrial Engineering. Marquette University. Currently: Aerothermal Engineer, Heat Transfer and Secondary Flow Systems, Turbine Module Center, Pratt & Whitney, East Hartford, CT. Member AIAA.
†Jack D. Whitfield Professor of High Speed Flows, Department of Mechanical, Aerospace and Biomedical Engineering. Member AIAA.

From a historical perspective, the bidirectional vortex concept applied to engines today was first implemented in industrial cyclones. In fact, one of the earliest analyses may be traced back to ter Linden's experimental work on dust separators in the late 1940s.[23] Both hydraulic and gas cyclones were later investigated by Kelsall[24] and Smith,[25,26] respectively.

For the conical cyclone, the earliest work may be attributed to Fontein and Dijksman[27] who once evoked semi-empirical approaches and curve fitting.[27] A more refined model based on the Polhausen method was later suggested by Bloor and Ingham[28] and shown to be in fair agreement with Kelsall's measurements.[24] A more useful approximation for the conical cyclone would later emerge from the work of Bloor and Ingham;[29] this time, they were able to incorporate realistic boundary conditions into their inviscid model. At the outset, their solution was quite useful in reproducing the overall features of the flow simulated numerically by Hsieh and Rajamani,[30] Hoekstra, Derksen and Van den Akker,[31] and Derksen and Van den Akker.[32] Bloor and Ingham's inviscid solution was singular at the core (as it relied on a free vortex) and assumed a constant product of the mean flow vorticity and chamber radius.[29]

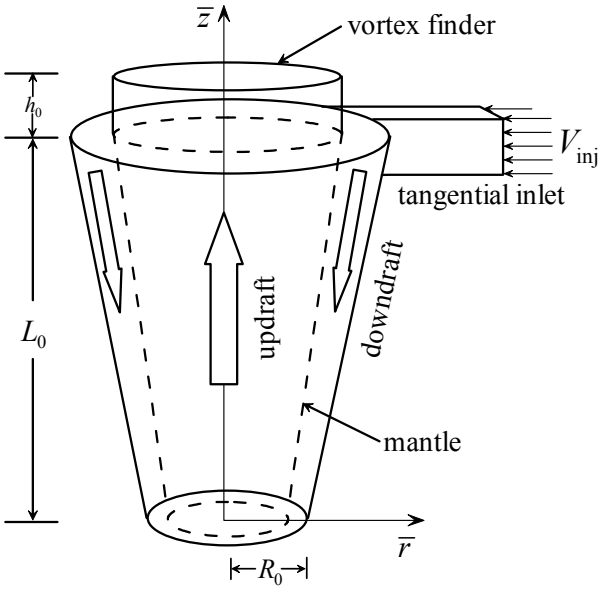

Figure 1. Schematic of typical cyclone separator.

Other studies, such as those by Zhao and Abrahamson,[33] sought to demonstrate the effect of the upstream boundary conditions in the presence of a vortex finder. Consideration was also given to the differences between axial and slotted injection. While some numerical studies explored the effect of geometry on the separation efficiency and performance of cyclone separators,[23] others sought to analyze the stability of swirling flows.[25,26]

Considering that the conical chamber is of key relevance to both industrial cyclones and modern concepts of liquid and hybrid engines, it is the purpose of this paper to construct an asymptotic solution for the bidirectional vortex in a conical setting. Our approach will rely on regular perturbations in the invariably small cone half angle and combine the methodologies used by Vyas, Majdalani and Chiaverini,[9] and Sams, Majdalani, and Flandro.[34]

II. Mathematical Model

The idealized cyclonic separator is characterized as a cylindrical, divergent circular-port chamber with a circumferential surface oriented at an angle α. The model presented here in Fig. 1 incorporates both the divergent and non-divergent geometries. The origin of the coordinate system of interest is expediently placed at the base of the device where $\bar{z}$ and $\bar{r}$ denote the axial and radial coordinates, respectively. The cylindrical section (the vortex finder) of the device has dimensions of length h_0 and radius R_0 and the conical segment has a dimensional height of L_0. For the model proposed, the flow can be characterized as (i) steady, (ii) inviscid, (iii) incompressible, (iv) rotational, and (v) non-reactive. In accordance with the stated assumptions, the equations of motion can be written as

$$\frac{1}{\bar{r}}\frac{\partial\left(\bar{r}\bar{u}_r\right)}{\partial\bar{r}}+\frac{1}{\bar{r}}\frac{\partial\bar{u}_\theta}{\partial\theta}+\frac{\partial\bar{u}_z}{\partial\bar{z}}=0 \tag{1}$$

for continuity; in turn, Euler's equations can be expressed as:

$$\bar{u}_r\frac{\partial\bar{u}_r}{\partial\bar{r}}+\frac{\bar{u}_\theta}{\bar{r}}\frac{\partial\bar{u}_r}{\partial\theta}+\bar{u}_z\frac{\partial\bar{u}_r}{\partial\bar{z}}-\frac{\bar{u}_\theta^{\,2}}{\bar{r}}=-\frac{1}{\bar{\rho}}\frac{\partial\bar{p}}{\partial\bar{r}} \tag{2}$$

$$\bar{u}_r\frac{\partial\bar{u}_\theta}{\partial\bar{r}}+\frac{\bar{u}_\theta}{\bar{r}}\frac{\partial\bar{u}_\theta}{\partial\theta}+\bar{u}_z\frac{\partial\bar{u}_\theta}{\partial\bar{z}}+\frac{\bar{u}_\theta\bar{u}_r}{\bar{r}}=-\frac{1}{\bar{\rho}\bar{r}}\frac{\partial\bar{p}}{\partial\theta} \tag{3}$$

$$\bar{u}_r\frac{\partial\bar{u}_z}{\partial\bar{r}}+\frac{\bar{u}_\theta}{\bar{r}}\frac{\partial\bar{u}_z}{\partial\theta}+\bar{u}_z\frac{\partial\bar{u}_z}{\partial\bar{z}}=-\frac{1}{\bar{\rho}}\frac{\partial\bar{p}}{\partial\bar{z}} \tag{4}$$

At this point, it is useful to make simplifications based on qualitative information that is ascertained from the physics of the problem. Pertaining to inviscid flows, a common generalization is that of axisymmetry. As usual,[29] one may also assume that the azimuthal velocity is independent of the axial coordinate. This is realized due to momentum conservation in the axial direction. Applying these generalizations to Eqs. (1)–(4), one obtains

$$\frac{1}{\overline{r}}\frac{\partial\left(\overline{r}\overline{u}_r\right)}{\partial\overline{r}}+\frac{\partial\overline{u}_z}{\partial\overline{z}}=0 \tag{5}$$

$$\overline{u}_r\frac{\partial\overline{u}_r}{\partial\overline{r}}+\overline{u}_z\frac{\partial\overline{u}_r}{\partial\overline{z}}-\frac{\overline{u}_\theta^{\,2}}{\overline{r}}=-\frac{1}{\overline{\rho}}\frac{\partial\overline{p}}{\partial\overline{r}} \tag{6}$$

$$\overline{u}_r\frac{\partial\overline{u}_\theta}{\partial\overline{r}}+\frac{\overline{u}_\theta\overline{u}_r}{\overline{r}}=0 \tag{7}$$

$$\overline{u}_r\frac{\partial\overline{u}_z}{\partial\overline{r}}+\overline{u}_z\frac{\partial\overline{u}_z}{\partial\overline{z}}=-\frac{1}{\overline{\rho}}\frac{\partial\overline{p}}{\partial\overline{z}} \tag{8}$$

Furthermore, the vorticity may be expressed in terms of the Stokes streamfunction following Culick,[35] and others;[9] as usual, one gets

$$-\overline{\Omega}_\theta=\frac{1}{\overline{r}}\frac{\partial^2\overline{\psi}}{\partial\overline{z}^2}+\frac{\partial}{\partial\overline{r}}\left(\frac{1}{\overline{r}}\frac{\partial\overline{\psi}}{\partial\overline{r}}\right) \tag{9}$$

The importance of this relationship will be soon established.

A. Boundary Conditions

The physical constraints are the same as those alluded to by Vyas, Majdalani and Chiaverini[9-11] in their seminal work on the bidirectional vortex in a cylindrical liquid rocket engine. They are: (i) tangential flow; (ii) no flow across the centerline; (iii) uniform, constant, tangential injection of fluid; (iv) no radial inflow along the walls of the device; and (v) mass balance requiring that the inflow be equal to the outflow at the lid of the separator. Mathematically, the boundary conditions are expressed in cylindrical coordinates. These constraints may be stated as

$$\begin{cases}\overline{r}=r_{\rm w},\ \overline{z}=L_0,\ \overline{u}_\theta=V_{\rm inj}\ \text{(uniform tangential injection)}\\ \overline{z}=0,\ \forall\overline{r},\ \overline{u}_z=0\ \text{(no flow through the base)}\\ \overline{r}=0,\ \forall\overline{z},\ \overline{u}_r=0\ \text{(no flow across the centerline)}\\ \overline{r}=r_{\rm w},\ 0\le\overline{z}<L,\ \overline{u}_r\cos\alpha-\overline{u}_z\sin\alpha=0\ \text{(no radial flow through the sidewall)}\\ \overline{z}=L,\ 0\le\overline{r}<b,\ \overline{Q}_{\rm o}=\overline{Q}_{\rm i}=V_{\rm inj}A_{\rm i}\ \text{(mass balance at the lid of the separator)}\end{cases} \tag{10}$$

where $V_{\rm inj}$ represents the injection velocity.

B. Normalization

Normalization can be accomplished by setting

$$z=\frac{\overline{z}}{R_0};\ r=\frac{\overline{r}}{R_0};L=\frac{L_0}{R_0};\ \nabla=R_0\overline{\nabla} \tag{11}$$

$$u_z=\frac{\overline{u}_z}{V_{\rm inj}};\ u_r=\frac{\overline{u}_r}{V_{\rm inj}};\ p=\frac{\overline{p}}{\rho V_{\rm inj}^2} \tag{12}$$

$$p=\frac{\overline{p}}{\rho V_{\rm inj}^2};\ Q_{\rm i}=\frac{\overline{Q}_{\rm i}}{V_{\rm inj}R_0^2}=\frac{A_{\rm i}}{R_0^2};\ Q_{\rm o}=\frac{\overline{Q}_{\rm o}}{V_{\rm inj}R_0^2};\ \ \psi=\frac{\overline{\psi}}{R_0V_{\rm inj}};\ \Omega=\frac{R_0\overline{\Omega}}{V_{\rm inj}} \tag{13}$$

Following suit, the normalized boundary conditions become

$$u_\theta(r_{\rm w},l)=1;\ \ u_z(r,0)=0;\ u_r(0,z)=0;\ \ u_r(r_{\rm w},z)\cos\alpha-u_z(r_{\rm w},z)\sin\alpha=0;\ Q_{\rm o}=\int_0^{2\pi}\int_0^{\eta}\boldsymbol{u}(r,l)\cdot\hat{\boldsymbol{n}}\,r\,{\rm d}r\,{\rm d}\theta=Q_{\rm i} \tag{14}$$

C. Free Vortex Solution

As a first approximation, one can extract a simple solution from the $\theta-$ momentum equation. The reduced equation begets

$$u_r\left(\frac{\partial u_\theta}{\partial r}+\frac{u_\theta}{r}\right)=0 \text{ or } u_\theta = A/r \tag{15}$$

Next, the boundary condition $u_\theta(r_w, L)=1$ yields

$$u_\theta = \frac{1+L\tan\alpha}{r} \tag{16}$$

When the angle of divergence is set to zero, this expression becomes identical to the free vortex distribution obtained for the cyclone in a straight cylinder.[9]

III. Methodology

To obtain the average velocity of the fluid in the conical domain, a mass balance is performed over a specified control volume. Essential to this development is how one chooses to characterize the bulk fluid motion within the control volume.

A. One-Dimensional Velocity

The conical geometry is based on the cylindrical coordinate system (as depicted in Fig. 1 where $\bar{z}$ is the dimensional axial coordinate and $\bar{r}$ is the dimensional radial coordinate). The surface area of the conical walls is given by

$$A_{\text{sf}} = 2\pi\left(R_0+\tfrac{1}{2}\bar{z}\tan\alpha\right)\bar{z}\sec\alpha \tag{17}$$

and the cross-sectional area may be evaluated from

$$A(\bar{z}) = \pi\left(R_0+\bar{z}\tan\alpha\right)^2 \tag{18}$$

$$\bar{u}_{\text{ave}}(\bar{z}) = \frac{A_{\text{sf}}V_{\text{inj}}}{A(\bar{z})} \tag{19}$$

By substituting Eqs. (17) and (18) into Eq. (19), the resulting relation may be expressed in normalized variables to obtain

$$u_{\text{ave}}(z) = \frac{2z\sec\alpha\left(1+\frac{1}{2}z\tan\alpha\right)}{\left(1+z\tan\alpha\right)^2} \tag{20}$$

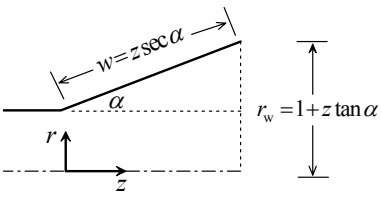

Figure 2. Wall coordinates.

B. Streamfunction at the Wall

Ascertaining the required form of the chamber vorticity is integral to the development of a flowfield that describes the fluid motion in a cyclone separator. Therefore, it is important to determine the behavior of the general streamfunction along the walls of the device. Accordingly, the directional derivative along the conical walls can be written as

$$\frac{\mathrm{d}\psi_{\text{w}}}{\mathrm{d}w} = \frac{\partial\psi}{\partial z}\cos\alpha+\frac{\partial\psi}{\partial r}\sin\alpha \tag{21}$$

Along the wall of the separator, the normalized global variables are evaluated to be

$$z = w\cos\alpha \qquad r_{\text{w}} = 1+w\sin\alpha \tag{22}$$

where the subscript ‘ w ’ denotes the direction parallel to the wall and w the corresponding coordinate (see Fig. 2). At this juncture, we switch our attention to a control volume formulation that may be used as a first approximation. Knowing that flow is steadily injected from the outer vortex into the inner vortex (across the mantle), we assume that there is mass flow entering through the control surfaces, thus leading to a general expression that relates the streamfunction at the wall, vorticity, and the velocity components in the given geometry. We therefore permit inflow at the control surface to deduce the general behavior of the vorticity. Since the crossflow simulates injection normal to the mantle location, we let

$$u_z = \sin\alpha \qquad u_r = -\cos\alpha \text{ (crossflow)} \tag{23}$$

Making use of the Stokes streamfunction relations, one can put

$$u_z = \frac{1}{r}\frac{\partial\psi}{\partial r}, \quad u_r = -\frac{1}{r}\frac{\partial\psi}{\partial z} \tag{24}$$

Substituting these expressions into Eq. (21) yields

$$\frac{\mathrm{d}\psi_{\mathrm{w}}}{\mathrm{d}w} = -r\left(\cos^2\alpha + \sin^2\alpha\right) \text{ or } \frac{\mathrm{d}\psi_{\mathrm{w}}}{\mathrm{d}w} = -\left(1 + w\sin\alpha\right) \tag{25}$$

Integrating the resulting expression and converting back to global coordinates, one is left with

$$\psi_{\mathrm{w}}\left(w\right) = -(w + \tfrac{1}{2}w^2\sin\alpha) \text{ or } \psi_{\mathrm{w}}\left(z\right) = -z\sec\alpha(1 + \tfrac{1}{2}z\tan\alpha) + C \tag{26}$$

where C is a constant that can be evaluated by applying the boundary condition, $\psi_{\mathrm{w}}\left(0\right) = 0$ (zero mass flux at the base). As a result, the closed-form streamfunction along the wall is arrived at; this is

$$\psi_{\mathrm{w}}\left(z\right) = -z\sec\alpha\left(1 + \tfrac{1}{2}z\tan\alpha\right) \tag{27}$$

C. Axial Pressure Gradient

A close examination of the fluid behavior suggests that the axial pressure gradient is the primary source of vorticity and aids in its transport along the streamlines. Thus, it is advantageous to exploit the relationship between the pressure gradient and the vorticity. One may start by expressing Bernoulli's equation along the central streamline by using

$$p(z) = p_0 - \tfrac{1}{2}u_{\max}^2(z) \tag{28}$$

Considering that the maximum velocity is unknown at the core of the cyclone, one may define a ratio between the maximum and average local velocities at any axial location z. This velocity ratio can be written as

$$\xi\left(z\right) = \frac{u_{\max}\left(z\right)}{u_{\mathrm{ave}}\left(z\right)} \tag{29}$$

The form of $\xi\left(z\right)$ will be later determined such that the no-slip condition in the direction parallel to the mantle is satisfied. Note that the mantle, or spinning (conical) wheel, is the surface along which only perpendicular crossflow is permitted from the downdraft to the updraft (see Fig. 1). By substituting Eq. (29) into Eq. (28), the expression becomes

$$p\left(z\right) = p_0 - \tfrac{1}{2}\xi^2 u_{\mathrm{ave}}^2\left(z\right) \tag{30}$$

The pressure gradient can be determined along the surface by calculating the derivative of Eq. (30). The result is

$$\frac{\mathrm{d}p}{\mathrm{d}z} = -\xi^2\left(z\right)u_{ave}\left(z\right)\left[\frac{\mathrm{d}u_{ave}\left(z\right)}{\mathrm{d}z} + \frac{u_{ave}\left(z\right)}{\xi\left(z\right)}\frac{\mathrm{d}\xi\left(z\right)}{\mathrm{dz}}\right] \tag{31}$$

Differentiating Eq. (20) and substituting the known quantities at the wall, one obtains

$$\frac{\mathrm{d}u_{\mathrm{ave}}}{\mathrm{dz}} = 2\frac{\sec\alpha}{r_{\mathrm{w}}} + 4\frac{\psi_{\mathrm{w}}\tan\alpha}{r_{\mathrm{w}}^3} \tag{32}$$

Finally, inserting Eq. (32) into Eq. (31) and simplifying, it follows that

$$\frac{\mathrm{d}p}{\mathrm{d}z} = 4\xi^2\frac{\psi_{\mathrm{w}}\sec\alpha}{{r_{\mathrm{w}}}^3}\left[1 + 2\frac{\psi_{\mathrm{w}}\sin\alpha}{{r_{\mathrm{w}}}^2} - \frac{\psi_{\mathrm{w}}\cos\alpha}{r_{\mathrm{w}}}\left(\frac{\xi'}{\xi}\right)\right];\ \xi' = \frac{\mathrm{d}\xi}{\mathrm{dz}} \tag{33}$$

D. Surface Vorticity

At this point, the momentum equation for steady, inviscid flow can be evaluated at the wall. Recalling the normalized form of Euler's momentum equation for steady, incompressible and inviscid flow, one may write

$$\boldsymbol{u}\cdot\nabla\boldsymbol{u} = -\nabla p \tag{34}$$

one may substitute the identity, $\boldsymbol{u}\cdot\nabla\boldsymbol{u} = \nabla\left(\tfrac{1}{2}\boldsymbol{u}\cdot\boldsymbol{u}\right) - \boldsymbol{u}\times\nabla\times\boldsymbol{u}$ to obtain an alternate expression of the form

$$\boldsymbol{u}\times\boldsymbol{\Omega} = \nabla\left(p + \tfrac{1}{2}\boldsymbol{u}\cdot\boldsymbol{u}\right) \tag{35}$$

The virtual velocity vector at the wall is defined as

$$\boldsymbol{u} = \sin\alpha\hat{i} - \cos\alpha\hat{j} \tag{36}$$

Evaluating the expression by substitution of Eq. (36) into Eq. (35) gives

$$\boldsymbol{u}\times\boldsymbol{\Omega} = -\boldsymbol{\Omega}_{\mathrm{w}}\left(\sin\alpha\hat{i} - \cos\alpha\hat{j}\right) = -\boldsymbol{\Omega}_{\mathrm{w}}\hat{\boldsymbol{w}} \tag{37}$$

where $\hat{\boldsymbol{w}}$ represents the unit vector parallel to the diverging wall. The relationship between the pressure gradient and the vorticity is now at hand. The pressure gradient parallel to the wall is treated in the same manner. One can put

$$\frac{\mathrm{d}p}{\mathrm{d}w}\hat{\boldsymbol{w}} = \left(\frac{\mathrm{d}p}{\mathrm{d}z}\cos\alpha + \frac{\mathrm{d}p}{\mathrm{d}r}\sin\alpha\right)\hat{\boldsymbol{w}} \tag{38}$$

Equating the expressions provided by Eqs. (37) and (38) gives

$$\Omega_{\mathrm{w}} = -\frac{\mathrm{d}p}{\mathrm{d}z}\cos\alpha - \frac{\mathrm{d}p}{\mathrm{d}r}\sin\alpha \tag{39}$$

Considering conical half angles of α between 6 and 20 degrees, the term containing $\sin\alpha$ is considered negligible. Taking this into account, Eq. (39) can be reduced to

$$\Omega_{\mathrm{w}} = -\frac{\mathrm{d}p}{\mathrm{d}z}\cos\alpha + O\left(\sin\alpha\right) \tag{40}$$

With a formulation for the pressure gradient at hand, the vorticity at the walls can be expressed as

$$\Omega_{\mathrm{w}} = -4\beta^2\frac{\psi_{\mathrm{w}}}{{r_{\mathrm{w}}}^3}\left[1 + 2\frac{\psi_{\mathrm{w}}\sin\alpha}{{r_{\mathrm{w}}}^2} - \frac{\psi_{\mathrm{w}}\cos\alpha}{r_{\mathrm{w}}}\left(\frac{\beta'}{\beta}\right)\right] \tag{41}$$

In the absence of sources in a steady, frictionless domain, one may use Crocco's theorem; accordingly, vorticity traveling along a (steady) streamline cannot be subject to attenuation. By equating the chamber vorticity to the vorticity at the wall, one obtains

$$\Omega(\psi, r) = (r / r_{\mathrm{w}})\Omega_{\mathrm{w}}(\psi, r) \tag{42}$$

Substituting Eq. (41) into Eq. (42) renders

$$\Omega = -4\xi^2 r\frac{\psi}{{r_{\mathrm{w}}}^4}\left[1 + 2\frac{\psi\sin\alpha}{{r_{\mathrm{w}}}^2} - \frac{\psi\cos\alpha}{r_{\mathrm{w}}}\left(\frac{\xi'}{\xi}\right)\right] \tag{43}$$

Since vorticity is preserved along the streamlines, the subscript may be dropped so long as one assumes motion along a streamline.

IV. Solution

With the derivation of the chamber vorticity now complete, one may equate Eq. (9) with Eq. (43) to precipitate a partial, nonlinear differential equation that governs the flow. Doing so, one obtains

$$\frac{\partial^2\psi}{\partial z^2} + \frac{\partial^2\psi}{\partial r^2} - \frac{1}{r}\frac{\partial\psi}{\partial r} = -4\xi^2 r^2\frac{\psi}{r_{\mathrm{w}}^4}\left[1 + 2\frac{\psi\sin\alpha}{r_{\mathrm{w}}^2} - \frac{\psi\cos\alpha}{r_{\mathrm{w}}}\left(\frac{\xi'}{\xi}\right)\right] \tag{44}$$

Following Clayton,[36] or Sams, Majdalani and Flandro,[34] one can obtain a PDE that is identical to that derived for the case of solid rocket motors with tapered bores. Given the small conical angles, the use of this method has furnished an equation that explicitly describes the chamber vorticity. In his study, Clayton[36] numerically determined the magnitudes of the axial derivatives of the streamfunction and their corresponding velocity ratios. As a result, he concluded that the axial derivatives were negligibly small. In particular, he noted that the terms ξ' and $\partial^2\psi/\partial z^2$ were small quantities (the focus here will be on the velocity ratio since the axial derivative of the streamfunction is needed to apply the boundary condition at the chamber base). We thus assume (and later verify) that the axial derivatives are so small that they can be ignored in the prescribed conical domain. Once the proper form of the velocity ratio has been obtained, a scaling analysis will be needed to justify neglecting ξ'. Using Clayton's arguments regarding the numerical analysis, one can reduce Eq. (44) into

$$\frac{\partial^2\psi}{\partial z^2} + \frac{\partial^2\psi}{\partial r^2} - \frac{1}{r}\frac{\partial\psi}{\partial r} = -4\xi^2 r^2\frac{\psi}{r_{\mathrm{w}}^4}\left(1 + 2\frac{\psi\sin\alpha}{r_{\mathrm{w}}^2}\right) \tag{45}$$

Since the governing equation is nonlinear, the method of regular perturbations will be used. To this end, the streamfunction and corresponding velocity can be expanded according to

$$\psi = \psi_0 + \psi_1\varepsilon + O\left(\varepsilon^2\right) \tag{46}$$

$$u_{\mathrm{w}} = u_{\mathrm{w},0} + u_{\mathrm{w},1}\varepsilon + O\left(\varepsilon^2\right) \tag{47}$$

Equation (29) can also be expanded in an effort to assure satisfaction of the no-slip condition along the wall; one writes

$$\xi = \xi_0 + \xi_1\varepsilon + \xi_2\varepsilon^2 + O\left(\varepsilon^3\right) \tag{48}$$

The perturbation parameter ε is due to the small conical half angle, namely,

$$\varepsilon = \sin\left(\alpha\right) \tag{49}$$

The governing equation can now be solved by first inserting Eq. (46) and Eq. (48) into Eq. (45) and expanding the resulting terms.

A. Basic Solution

For the sake of brevity, the details of the expansion are not presented here. At leading order, one collects

$$\frac{\partial^2\psi_0}{\partial z^2} + \frac{\partial^2\psi_0}{\partial r^2} - \frac{1}{r}\frac{\partial\psi_0}{\partial r} = -4\xi_0^2 r^2\frac{\psi_0}{r_{\mathrm{w}}^4} \tag{50}$$

At this juncture, a general solution may be sought using variation of parameters. Accordingly, an arbitrary solution may be expressed as

$$\psi_0\left(z,r\right) = C_1\left(z\right)\sin\left(\xi_0\frac{r^2}{r_{\mathrm{w}}^2}\right) + C_2\left(z\right)\cos\left(\xi_0\frac{r^2}{r_{\mathrm{w}}^2}\right) \tag{51}$$

Inserting Eq. (51) into Eq. (50), one finds

$$\psi_0\left(z,r\right) = \left(K_1 z + K_2\right)\sin\left(\xi_0\frac{r^2}{r_{\mathrm{w}}^2}\right) + \left(K_3 z + K_4\right)\cos\left(\xi_0\frac{r^2}{r_{\mathrm{w}}^2}\right) \tag{52}$$

With a general solution at hand, one may now apply the required boundary conditions. Axisymmetry reduces Eq. (52) to

$$\psi_0\left(z,r\right) = \left(K_1 z + K_2\right)\sin\left(\xi_0\frac{r^2}{r_{\mathrm{w}}^2}\right) \tag{53}$$

Next, the condition at the base of the device yields

$$u_z = \frac{1}{r}\frac{\partial\psi_0\left(0,r\right)}{\partial r}\bigg|_{\forall r} = 0 \ \text{ or } \ K_2 = 0 \tag{54}$$

Application of the impermeability condition along the diverging wall gives

$$u_r = -\frac{1}{r_{\mathrm{w}}}\frac{\partial\psi_0\left(z,r_{\mathrm{w}}\right)}{\partial z}\bigg|_{\forall z}\cos\alpha = 0 \ \text{ or } \ \frac{K_1}{r_{\mathrm{w}}}\sin\left(\xi_0\right) = 0; \quad \xi_0 = n\pi,\ n = 1 \tag{55}$$

The last constant of integration K_1 can be determined by matching the inflow-outflow condition $\left(Q_{\mathrm{o}} = Q_{\mathrm{i}}\right)$ at the lid of the separator.[9] Recalling the outflow condition at the lid, one may set

$$Q_{\mathrm{o}} = \int_0^{2\pi}\int_0^{\eta}\boldsymbol{u}\left(r,L\right)\cdot\hat{\boldsymbol{n}}\ r\mathrm{d}r\mathrm{d}\theta = 2\pi\int_0^{\eta}u_z\left(r,L\right)r\mathrm{d}r \tag{56}$$

where $\eta = \tilde{\beta} + z\tan\gamma$ defines the radial location of the mantle at any axial location in the chamber and $\tilde{\beta}$ is the location of the mantle at $\alpha = 0^{\circ}$. Consequently, the final constant of integration can be extracted; one gets

$$K_1 = \frac{Q_{\mathrm{i}}\csc\left[\pi\eta^2\left(z=L\right)\right]}{2\pi L} = \frac{Q_{\mathrm{i}}\csc\left[\frac{1}{2}\pi(1+L\tan\alpha)^2\right]}{2\pi L} \tag{57}$$

The expression for the leading order solution becomes

$$\psi_0\left(r,z\right) = \kappa z\sin\left(\xi_0\frac{r^2}{r_{\mathrm{w}}^2}\right) \tag{58}$$

where $\kappa = K_1$ is a global mass inflow constant. Here, it is seen that at $\alpha = 0^{\circ}$ and $\eta = \tilde{\beta}$, the leading order solution reduces to

$$\psi\left(r,z\right) = \kappa z\sin\left(\pi r^2\right) \tag{59}$$

Equation (59) is identical, as it should, to the bidirectional vortex profile in a cylinder.[9]

Having obtained the general form of the streamfunction, one may now examine the fluid dynamical characteristics in conical chambers. It is instructive to note that the quantities in question can be evaluated at leading order without any appreciable loss in concept. As will be seen in forthcoming sections, the basic solution distinctly captures the general behavior of the bulk flow particular to conical chambers with tangential injection.

B. Velocity

The axial and radial velocity components can be determined from the definition of the streamfunction. Forthwith, axial and radial velocities take the form

$$u_{z,0} = 2\xi_0 \kappa z r_{\mathrm{w}}^{-2} \cos\left(\xi_0 r^2 r_w^{-2}\right) + O(\varepsilon), \quad u_{r,0} = -(\kappa / r)\sin\left(\xi_0 r^2 r_{\mathrm{w}}^{-2}\right) + O(\varepsilon) \tag{60}$$

C. Theoretical Mantle Location

It is known that the mantle is a spinning, non-translating layer that physically separates the updraft from the downdraft. At the mantle, the physicality of the system requires that the axial velocity changes polarity, thus allowing the fluid to make its way toward the lid of the separator. In their recent work, Vyas, Majdalani and Chiaverini[9] successfully predicted the theoretical mantle location by analytical methods. The location of the mantle was found to be

$$\tilde{\beta} = 1/\sqrt{2} \simeq 0.707 \tag{61}$$

This value was obtained by determining the value of the normalized radial location for which $u_z = 0$. Their results were found to be in good agreement with current CFD results,[5] as well as the results from Smith's study of a cylindrical gas cyclone in which he obtained a value of 0.72, and those by Fang, Majdalani and Chiaverini[21,22] who reported an average value of 0.74 under cold flow conditions.

For the bidirectional vortex in a conical chamber, one may obtain the root required for zero axial velocity in the same manner. Thus, one may put

$$\cos\left(\xi_0 \frac{\tilde{\eta}^2}{r_{\mathrm{w}}^2}\right) = 0 \tag{62}$$

It is clear that the mantle in a conical chamber is angularly oriented. Since the mantle location changes with axial location, it is expedient to determine the magnitude of the mantle angle. Doing so, one may write

$$\frac{\tilde{\eta}^2}{r_{\mathrm{w}}^2} = \frac{1}{2} \;\Rightarrow\; \frac{\left(\tilde{\beta} + z\tan\gamma\right)^2}{\left(1 + z\tan\alpha\right)^2} = \frac{1}{2} \tag{63}$$

In order to find the mantle angle, γ, the relationship must be evaluated at $z = L$. At the outset, one extracts

$$\gamma = \tan^{-1}\left(\frac{1 + L\tan\alpha}{L\sqrt{2}} - \frac{\tilde{\beta}}{L}\right) = \tan^{-1}\left(\frac{\tan\alpha}{\sqrt{2}}\right) \simeq \frac{\tan\alpha}{\sqrt{2}} - \frac{\tan^3\alpha}{2\sqrt{2}} + O(\tan^5\alpha) \tag{64}$$

Clearly, the mantle angle depends on the cone angle independently of the height-to-radius ratio of the chamber. Note that $\gamma = 0$ is recovered, as expected, for a right cylinder representing a cone with zero divergence. Based on Eq. (64) one can recalculate the radial location of the mantle at any z location. One finds:

$$\eta = \tilde{\beta} + z\tan\gamma \;= (1 + z\tan\alpha)/\sqrt{2} \tag{65}$$

Note that, based on trigonometric identities, one can verify that $\tilde{\beta} = \tan\gamma / \tan\alpha = 1/\sqrt{2}$.

D. Pressure and Vorticity

Having determined the velocity fields in the conical chamber, the pressure gradients may be formulated by substituting the known velocity components into the axial and radial momentum equations, respectively. The axial pressure gradient becomes

$$-\frac{\partial p_0}{\partial z} = \frac{4\xi_0^2 \kappa^2 z}{r_{\mathrm{w}}^5} \tag{66}$$

Similarly, the radial pressure gradient may be written as

$$-\frac{\partial p_0}{\partial r} = \frac{\kappa^2}{r}\left[2\xi_0 \cos\left(\xi_0 \frac{r^2}{r_{\mathrm{w}}^2}\right) - \frac{1}{r^2}\sin^2\left(\xi_0 \frac{r^2}{r_{\mathrm{w}}^2}\right)\right] \tag{67}$$

By integrating and combining Eqs. (66) and (67), one is able to produce the spatial variation of the pressure that satisfies both momentum equations. Due to the bidirectional and conical nature of the flowfield, the radial pressure distribution is quite appreciable. At this point one may evaluate the vorticity in order to complete the extraction of the parameters that are most critical to our study. Using $\Omega_\theta(z,r) = \partial u_z / \partial r - \partial u_r / \partial z$, one may substitute the velocity components to get

$$\Omega_\theta = 4\xi_0^2 rz\kappa \sin\left(\xi_0 \frac{r^2}{r_w^2}\right) \tag{68}$$

This completes the leading order approximation for the conical bidirectional vortex flowfield.

V. Results and Discussion

Up to this point, we have obtained a solution in terms of the streamfunction. Using the classic relationship between the velocity and the streamfunction, the axial and radial pressure gradients were ascertained along with the spatial variation of the vorticity. In this section, plots of these typical fluid dynamical quantities are furnished.

A. Streamlines

Thus far, the quest for an intuitive understanding of the bidirectional fluid motion in conical chambers has led one to consider the streamlines. The streamlines depict the basic behavior of the fluid and provide valuable information regarding the flowfield gradients and their response to the change of polarity. As seen in Fig. 3, the streamlines are plotted for several cone angles and $L = 1$. From these graphs, it is clear that the fluid enters the conical chamber at the lid of the device, or more precisely, at $z = L$. It travels along a helical trajectory in the downward draft. Near the base of the device, the fluid makes a complete turn, and then courses its way back to the top. Larger cone angles cause a wider scatter between streamlines near the top of the separators; this is clearly a reflection of the slower axial speeds induced by an increasing flow area. This phenomenon is further supported by the fact that flow gradients decrease with increasing aspect ratios.

B. Velocity and Conical Mantle

So far, the axial, azimuthal and radial velocity components were approximated. In light of the flowfield in question, it is instructive to graphically examine each of the velocities as a means to confirm our intuitive generalizations about flowfields particular to conical chambers. Figure 4 illustrates the response of the axial velocity field to the change in cone angle. In particular, Fig. 4a shows the solution originally obtained by Vyas, Majdalani and Chiaverini,[9] in which the mantle (locus of zero velocity) remains at a constant value of 0.707 at all axial locations. Conversely, the mantle location in the conical chamber is oriented at an angle and assumes a different value at each axial location. By examining each of the plots, it may be seen that the point at which the polarity of the profile changes is a function of axial distance. This distance is accurately prescribed by Eq. (65). For example, using $L = 1$, $z = 0.75L$, $\alpha = 10^\circ$, one calculates $\gamma = 7.1^\circ$ and $\eta = 0.8$. This radial position of the mantle matches the point where the corresponding (dashed) line in Fig. 4b intersects the zero axis. Furthermore, one may infer that the core velocity must diminish to compensate for the gradual increase in cross-sectional area as the fluid is upward traveling. Thus, the maximum updraft velocity occurs at the smallest cone angle.

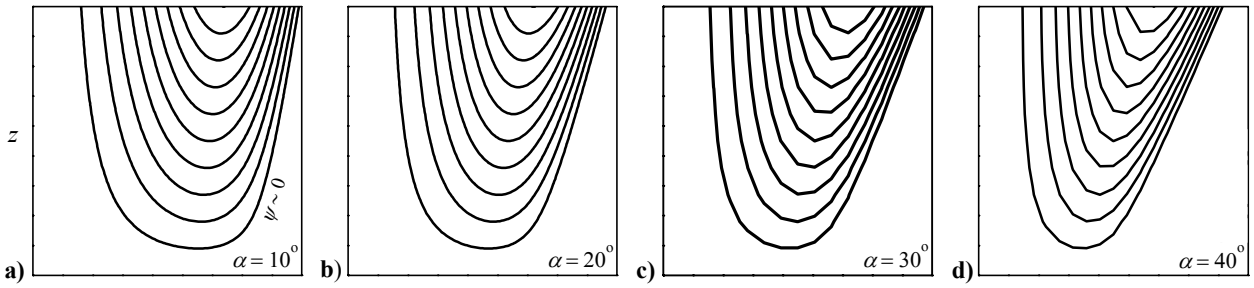

Figure 3. Streamline patterns for $L = 1$ and a) $\alpha = 10^o$, b) 20^o, c) 30^o, and d) 40^o.

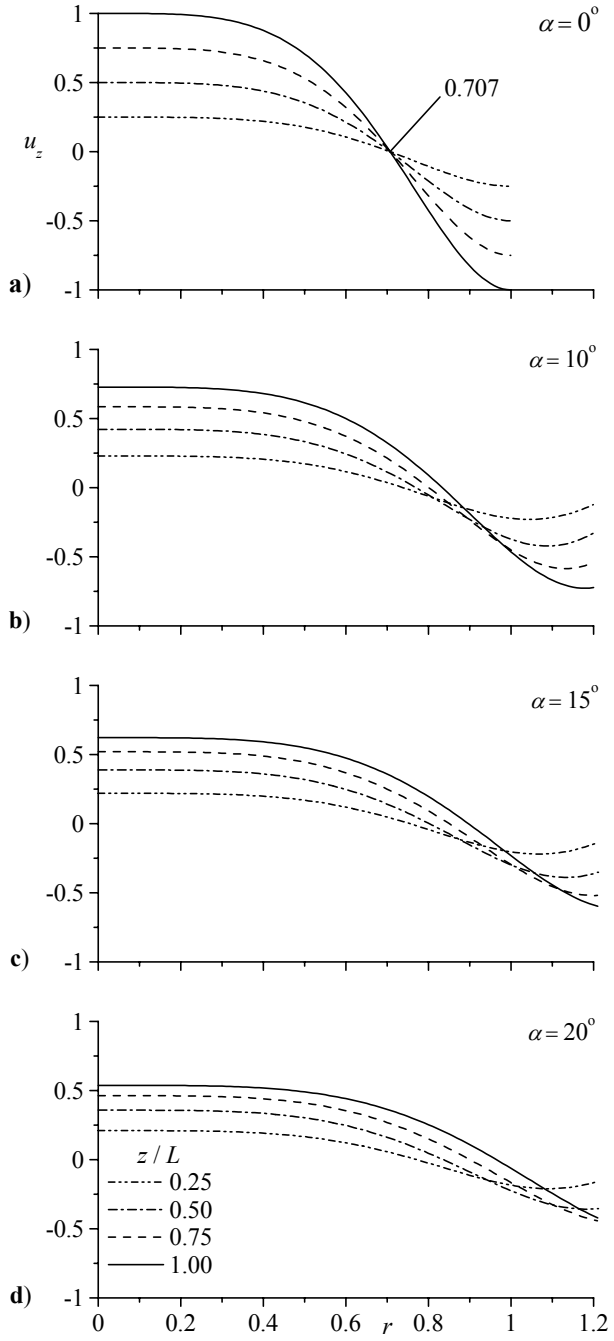

Figure 4. Streamwise velocity at several axial locations corresponding to a) $\alpha = 0^o$, b) 10^o, c) 15^o, and d) 20^o.

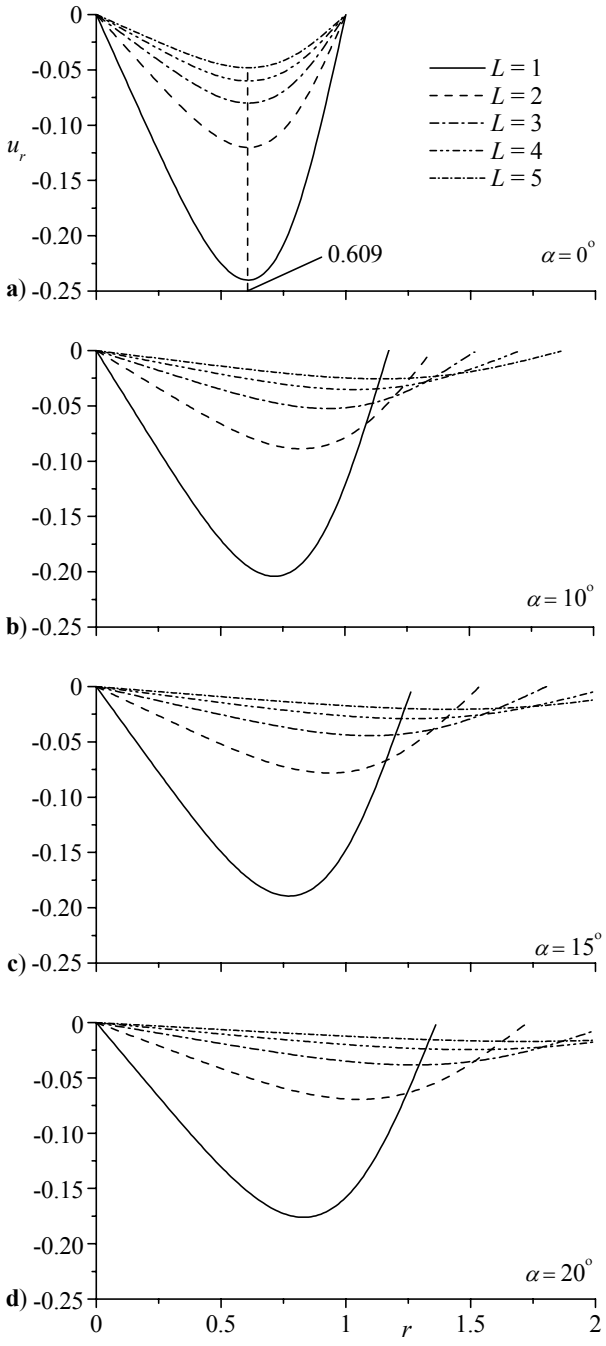

Figure 5. Radial velocity at several axial locations corresponding to a) $\alpha = 0^o$, b) 10^o, c) 15^o, and d) 20^o.

The radial velocity profiles are shown in Fig. 5 for various cone angles and several aspect ratios. Reminiscent of the radial profiles for the bipolar flowfield in a cylinder, the effect of aspect ratio is such that the maximum radial velocity is decreased as the aspect ratio is increased. For $\alpha = 0^\circ$, Vyas, Majdalani and Chiaverini[9] found the maximum radial velocity to occur near the mantle location. In Fig. 5, it can be seen that the radial location of maximum radial velocity shifts with the change in angular orientation, and the radial location at which the velocity recovers its zero value clearly increases with increasing cone angle. This is due to the increase in radial distance from the axis to the chamber wall.

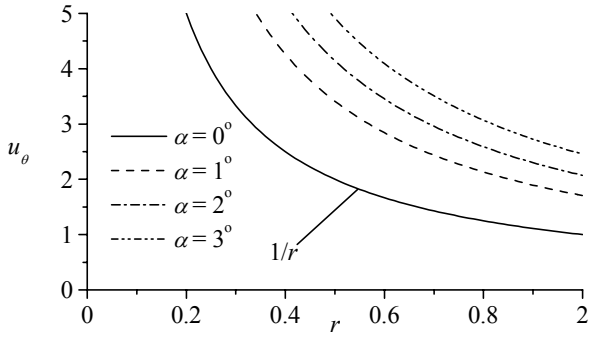

Figure 6. Azimuthal velocity component shown at several taper angles.

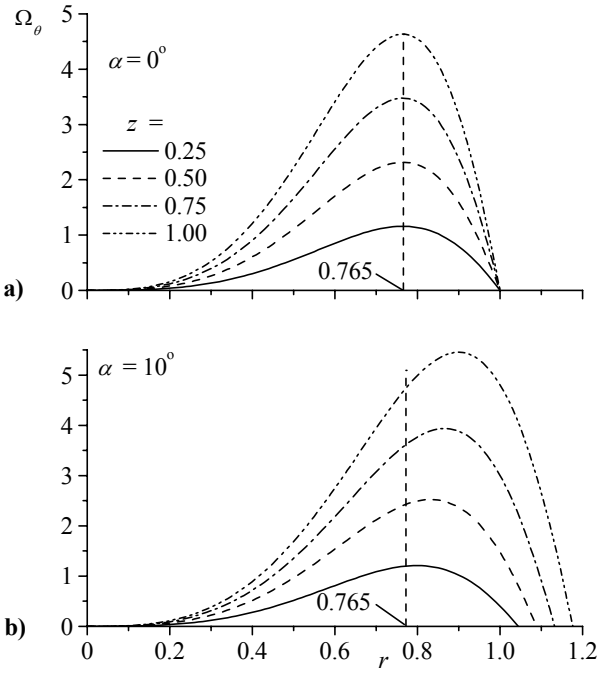

Figure 7. Radial variation of vorticity at several aspect ratios for a) $\alpha = 0^o$ and b) 10^o.

Shown in Fig. 6 is the azimuthal velocity component for $L = 4$ and several cone angles. Similar to the case for $\alpha = 0^\circ$, the value of the azimuthal velocity component approaches the value of the tangential velocity at the wall. One should also note that the no-slip condition is not satisfied at the chamber wall. This fact is due to the inviscid fluid assumption made during the derivation process. At the core, the velocity appears to be unbounded. This behavior is consistent with the classic assumption of a free vortex,[29] namely, one that is routinely used to decouple the momentum equations. Hence, one may expect a forced vortex at the core region in which the effects of viscosity become substantial. For $\alpha = 0^\circ$, Vyas, Majdalani and Chiaverini[10] accounted for these viscous effects by using matched asymptotic expansions to capture the boundary layer near the chamber axis. It is hoped that the core corrections for the conical cyclone will be analyzed in future studies.

C. Vorticity

In Fig. 7 it is clear that the behavior of the vorticity follows that of the radial velocity component. The vorticity seems to increase in a linear fashion and peaks between the mantle and the conical walls. As expected, the vorticity decays along the axis. The position at which maximum vorticity is attained changes with the cone angle. The position where vorticity is maximum at $\alpha = 0^\circ$ (for the baseline cylindrical cyclone) is shown on each plot as a means for comparison. The extreme positions seem to shift in a manner consistent with the behavior of the mantle for non-zero half angles.

D. Pressure Gradients

The pressure gradients are plotted in Figs. 8–9 in an effort to characterize the variation of the pressure gradient with the conical half angle. Typically, the gradients are integrated in order to obtain discrete values of pressure at any given point in the chamber. However, given the axial dependence of the chamber radius, the expression must be numerically integrated. In previous studies that have applied similar methodology,[37] the distance to the wall was assumed to be constant. Furthermore, the radial and transverse pressure terms were considered small and, therefore, neglected. This assumption allowed a closed-form expression for the total pressure drop to be obtained. In the case for the conical chamber, the radial pressure term is significant in determining the overall physics of the problem and becomes essential for studying the characteristics of industrial cyclones.

In Fig. 8 the axial pressure gradient is plotted in the axial direction at several cone angles. One can see that the behavior exhibited is reminiscent of the corresponding axial velocity profile. The change in flow area is obviously due to an increase in radial distance. The physics dictate that, with increasing radial distance in the axial direction, the downdraft moves closer to the wall, thus increasing the available flow area. As a result the velocity must decrease if mass continuity is to be satisfied. In this fashion, as the cone angle increases, diffusion causes the local velocity to depreciate and the static pressure to be higher at a given axial position; at the outset, the rate of change in pressure becomes less appreciable in the axial direction. One may realize that it approaches a constant value as the fluid moves toward the vortex finder.

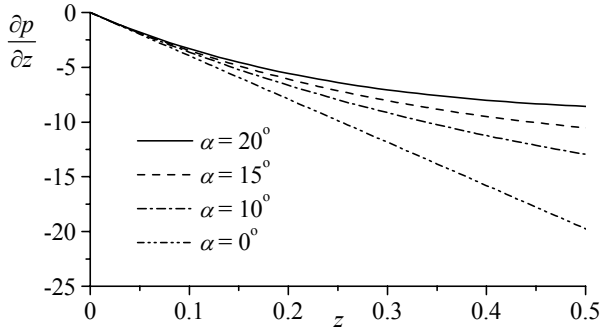

Figure 8. Axial pressure gradient at several taper angles.

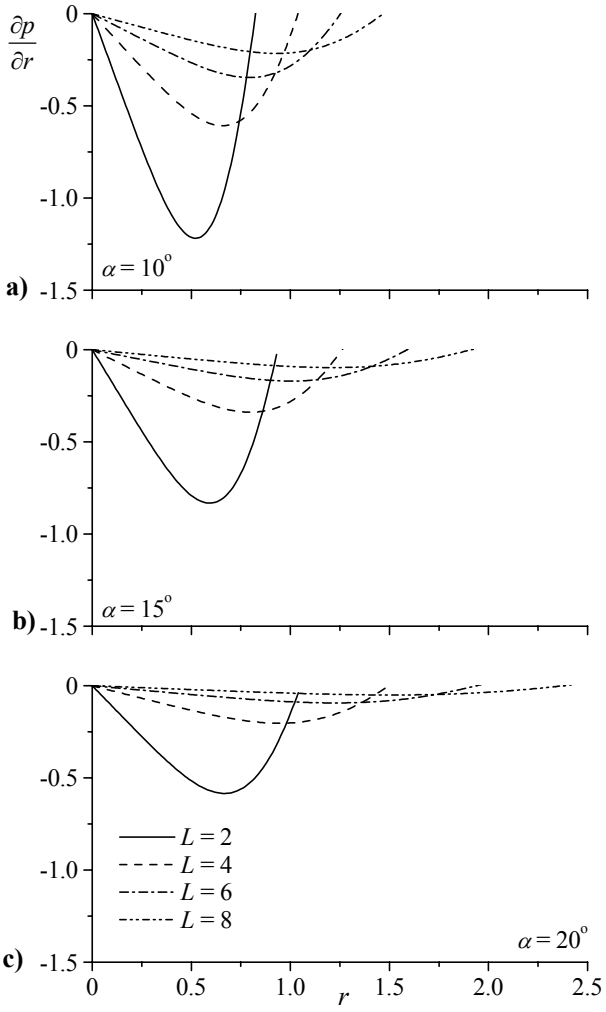

Figure 9. Radial pressure gradients at several aspect ratios and a) $\alpha = 10^o$, b) 15^o, and c) 20^o.

The behavior of the radial pressure gradient is illustrated in Fig. 9. Judging from the behavior of the radial velocity in the chamber, one would naturally expect the pressure gradient to behave in the same manner. The radial pressure gradient is an important mechanism in the operation of the cyclone. It is what drives the cross-flow allowing the finer particles to move into the updraft and forces the heavier particles to the wall of the device. The radial pressure gradient also reaches its peak between the mantle and the wall, as in the case for the injection-driven bidirectional flow in a cylinder.

VI. Concluding Remarks

This work has presented a basic approach to mathematically model bidirectional flow in conical chambers using a regular perturbation method. This approach has produced a flowfield that illustrates the bipolar behavior of an inviscid, rotational, incompressible fluid. In order to take advantage of the angular offset of the chamber walls and its effects on the chamber vorticity, an expression for the vorticity at the surface had to be obtained. This method produced an expression for the chamber vorticity in terms of the streamfunction. From the streamfunction, the key attributes of the flow could be assessed.

The velocity, vorticity and pressure were quantified and compared to the bidirectional vortex in a straight cylinder. One characteristic worth noting here is the angular offset of the mantle. This suggests that a similar offset will exist for the locus of zero vorticity, as well as the radial pressure. The location of the mantle may be useful in sizing vortex finders and maximizing separation efficiency. The analytical location of the maximum and minimum vorticities may be helpful in maximizing performance parameters and in designing cyclonic combustion engines.

Thus far, we have produced a solution that reflects the bidirectional behavior in conical chambers. Future work would involve a matched asymptotic treatment of the viscous core and a complete analysis of the angular locations for the extreme values of vorticity, velocity and pressure. The higher-order corrections for each fluid dynamical quantity must be determined and the Ekman-type boundary layers must be captured along the walls. It is quite possible that these corrections will yield valuable information about the characteristics of the flowfield in question. Finally, a comparable numerical solution would, in effect, enable us to gain confidence in the mathematical model put forth in this work. From the numerical solution, some of the generalizations and assumptions could be validated.

Acknowledgments

This work was sponsored by the National Science Foundation through Grant No. CMS-0353518, Program Manager, Dr. Masayoshi Tomizuka. The work of J. Majdalani was partially funded by the Jack D. Whitfield Professorship of High Speed Flows, University of Tennessee. The authors thank Dr. Martin J. Chiaverini of Orbital Technologies Corporation, Madison, WI, for various discussions in support of this effort and for promoting interest in vortex engine technology.

References

[1]Anderson, M. H., Valenzuela, R., Rom, C. J., Bonazza, R., and Chiaverini, M. J., "Vortex Chamber Flow Field Characterization for Gelled Propellant Combustor Applications," AIAA Paper 2003-4474, July 2003.

[2]Rom, C. J., Anderson, M. H., and Chiaverini, M. J., "Cold Flow Analysis of a Vortex Chamber Engine for Gelled Propellant Combustor Applications," AIAA Paper 2004-3359, July 2004.

[3]Chiaverini, M. J., Sauer, J. A., and Knuth, W. K., "Final Report on Vortex Combustion Combined Cycle Engine- a Phase I SBIR Project," Orbital Technological Corporation, Air Force Contract No. F04611-99-C-0063 Rept. OTC-GS082-FR-99-1, March 1999.

[4]Chiaverini, M. J., Malecki, M. J., Sauer, J. A., Knuth, W. H., and Hall, C. D., "Final Report on Cold-Wall Vortex Combustion Chamber-a Phase I SBIR Project," Orbital Technological Corporation, NASA Contact No. NAS8-01073 Rept. OTC-GS0107-01-1, August 2001.

[5]Chiaverini, M. J., Malecki, M. J., Sauer, J. A., and Knuth, W. H., "Vortex Combustion Chamber Development for Future Liquid Rocket Engine Applications," AIAA Paper 2002-2149, July 2002.

[6]Chiaverini, M. J., Malecki, M. M., Sauer, J. A., Knuth, W. H., and Hall, C. D., "Testing and Evaluation of Vortex Combustion Chamber for Liquid Rocket Engines," JANNAF 2002.

[7]Chiaverini, M. J., Malecki, M. J., Sauer, J. A., Knuth, W. H., and Majdalani, J., "Vortex Thrust Chamber Testing and Analysis for O2-H2 Propulsion Applications," AIAA Paper 2003-4473, July 2003.

[8]Sauer, J. A., Malecki, M. M., Knuth, W. H., Chiaverini, M. J., and Hall, C. D., "Development of a LOX/RP-1 Vortex Combustion Cold-Wall Thrust Chamber Assembly," AAIA Paper 2002-4144, July 2002.

[9]Vyas, A. B., Majdalani, J., and Chiaverini, M. J., "The Bidirectional Vortex. Part 1: An Exact Inviscid Solution," AIAA Paper 2003-5052, July 2003.

[10]Vyas, A. B., Majdalani, J., and Chiaverini, M. J., "The Bidirectional Vortex. Part 2: Viscous Core Corrections," AIAA Paper 2003-5053, July 2003.

[11]Vyas, A. B., Majdalani, J., and Chiaverini, M. J., "The Bidirectional Vortex. Part 3: Multiple Solutions," AIAA Paper 2003-5054, July 2003.

[12]Majdalani, J., and Vyas, A. B., "Rotational Axisymmetric Mean Flow for the Vortex Injection Hybrid Rocket Engine," AIAA Paper 2004-3475, July 2004.

[13]Knuth, W. H., Chiaverini, M. J., Sauer, J. A., and Gramer, D. J., "Solid-Fuel Regression Rate Behavior of Vortex Hybrid Rocket Engines," *Journal of Propulsion and Power,* Vol. 18, No. 3, 2002, pp. 600-609.

[14]Knuth, W. H., Chiaverini, M. J., Gramer, D. J., and Sauer, J. A., "Final Report on Gas-Fed, Vortex Injection Hybrid Rocket Engine- a Phase II SBIR Project," Orbital Technological Corporation, NASA Contract No. NAS8-97015 Rept. OTC-GS055-FR-99-1, Madison, Wisconsin, January 1999.

[15]Knuth, W. H., Chiaverini, M. J., Gramer, D. J., and Sauer, J. A., "Final Report on Vortex Combustion Ramjet- a Phase I SBIR Project," Orbital Technological Corporation, NASA Contract No. NAS3-99039 Rept. OTC-GS075-FR-99-1, June 1999.

[16]Knuth, W. H., Chiaverini, M. J., Gramer, D. J., and Sauer, J. A., "Solid-Fuel Regression Rate and Combustion Behavior of Vortex Hybrid Rocket Engines," AIAA Paper 99-2318, July 1999.

[17]Knuth, W. H., Chiaverini, M. J., Gramer, D. J., Sauer, J. A., St. Clair, C. P., Whitesides, R. H., and Dill, R. A., "Preliminary Computational Fluid Dynamics Analysis of the Vortex Hybrid Rocket Chamber and Nozzle Flowfield," AIAA Paper 98-3351, July 1998.

[18]Knuth, W. H., Gramer, D. J., Chiaverini, M. J., and Sauer, J. A., "Development and Testing of Vortex Driven, High Regression Rate Hybrid Rocket Engines," AIAA Paper 98-3507, July 1998.

[19]Knuth, W. H., Chiaverini, M. J., Gramer, D. J., and Sauer, J. A., "Experimental Investigation of a Vortex-Driven High-Regression Rate Hybrid Rocket Engine," AIAA Paper 98-3348, July 1998.

[20]Knuth, W. H., Bemowski, P. A., Gramer, D. J., Majdalani, J., and Rothbauer, W. J., "Gas-Fed, Vortex Injection Hybrid Rocket Engine," NASA Marshall Space Flight Center, SBIR Phase I Final Technical Rept. NASA/MSFC Contract NAS8-40679, Huntsville, AL, August 1996.

[21]Fang, D., Majdalani, J., and Chiaverini, M. J., "Simulation of the Cold-Wall Swirl Driven Combustion Chamber," AIAA Paper 2003-5055, July 2003.

[22]Fang, D., Majdalani, J., and Chiaverini, M. J., "Hot Flow Model of the Vortex Cold Wall Liquid Rocket," AIAA Paper 2004-3676, July 2004.

[23]ter Linden, A. J., "Investigations into Cyclone Dust Collectors," *Proceedings of the Institution of Mechanical Engineers,* Vol. 160, 1949, pp. 233-251.

[24]Kelsall, D. F., "A Study of Motion of Solid Particles in a Hydraulic Cyclone," *Transactions of the Institution of Chemical Engineers,* Vol. 30, 1952, pp. 87-103.
[25]Smith, J. L., "An Experimental Study of the Vortex in the Cyclone Separator," *Journal of Basic Engineering-Transactions of the ASME*, 1962, pp. 602-608.
[26]Smith, J. L., "An Analysis of the Vortex Flow in the Cyclone Separator," *Journal of Basic Engineering-Transactions of the ASME*, 1962, pp. 609-618.
[27]Fontein, F. J., and Dijksman, C., *Recent Developments in Mineral Dressing*, Institution of Mining and Metallurgy, London, 1953, p. 229.
[28]Bloor, M. I. G., and Ingham, D. B., "Theoretical Investigation of the Flow in a Conical Hydrocyclone," *Transactions of the Institution of Chemical Engineers,* Vol. 51, 1973, pp. 36-41.
[29]Bloor, M. I. G., and Ingham, D. B., "The Flow in Industrial Cyclones," *Journal of Fluid Mechanics,* Vol. 178, 1987, pp. 507-519.
[30]Hsieh, K. T., and Rajamani, R. K., "Mathematical Model of the Hydrocyclone Based on Physics of Fluid Flow," *AIChE Journal,* Vol. 37, No. 5, 1991, pp. 735-746.
[31]Hoekstra, A. J., Derksen, J. J., and Van den Akker, H. E. A., "An Experimental and Numerical Study of Turbulent Swirling Flow in Gas Cyclones," *Chemical Engineering Science,* Vol. 54, 1999, pp. 2055-2065.
[32]Derksen, J. J., and Van den Akker, H. E. A., "Simulation of Vortex Core Precession in a Reverse-Flow Cyclone," *AIChE Journal,* Vol. 46, No. 7, 2000, pp. 1317-1331.
[33]Zhao, J. Q., and Abrahamson, J., "The Flow in Industrial Cyclones," *Second International Conference on CFD in the Minerals and Process Industries, Melbourne Austraila,* Vol. December 6-8, 1999, 1999.
[34]Sams, O. C., Majdalani, J., and Flandro, G. A., "Higher Flowfield Approximations for Solid Rocket Motors with Tapered Bores," AIAA Paper 2004-4051, July 2004.
[35]Culick, F. E. C., "Rotational Axisymmetric Mean Flow and Damping of Acoustic Waves in a Solid Propellant Rocket," *AIAA Journal,* Vol. 4, No. 8, 1966, pp. 1462-1464.
[36]Clayton, C. D., "Flowfields in Solid Rocket Motors with Tapered Bores," AIAA Paper 96-2643, July 1996.
[37]Sams, O. C., Majdalani, J., and Flandro, G. A., "Slab Rocket Motor with Tapered Side Walls," AIAA Paper 2003-5114, July 2003.